International Journal of Power Electronics and Drive System (IJPEDS)
Vol. 8, No. 3, September 2017, pp. 1345~1358
ISSN: 2088-8694, DOI: 10.11591/ijpeds.v8i3.pp1345-1358

Sliding Mode Observers-based Fault Detection and Isolation for Wind Turbine-driven Induction Generator

T. Sellami[1], H. Berriri[2], S. Jelassi[3], A. M Darcherif[4] and M.F. Mimouni[5]
[1,2,4] Electrical Department, National Electrical Engineering Department of Engineering School of Monastir
[1,2,5] Engineering Department, Cergy-Pontoise University

Article Info

Article history:

Received Mar 17, 2017
Revised Jun 20, 2017
Accepted Aug 10, 2017

Keyword:

Fault detection and isolation
Inter-turn short-circuit fault
Residuals
Sliding mode observer
Thresholds
Wind turbine driven induction generator

ABSTRACT

Inter-turn short-circuit (ITSC) faults on the induction machine has received much attention in the recent years. Early detection of such faults in wind turbine systems would allow to avoid fluctuation on wind power outputand maintain the reliability level. In this paper, Sliding Mode Observers (SMO)-based fault detection and isolation method is developed for induction generator (IG)-based variable-speed grid-connected wind turbines. Firstly, the dynamic model of the wind turbine and IG was given and then, the control was made based on Maximum Power Point Tracking (MPPT) method. The IG closed-loop via Indirect Rotor Flux Oriented Control (IRFOC) scheme was also described. Hence, the performance of the wind turbine system and the stability of injected power to the grid were analyzed under the ITSC fault conditions. The control schemeswere proved to be inherently unstable under the faulty conditions. Then, robust SMO were investigated to design an ITSC fault detection and isolation scheme. Finally, simulation results of ITSC detection and isolation in the variable-speed grid-connected wind turbine with affected IG confirm the theoretical development.

Corresponding Author:

Takwa Sellami**,**
Quartz-Lab, EA 9373, Engineering Department and ESIER, Electrical Department
Cergy-Pontoise University, Cergy 95000, France and ENIM, Monastir 5000, Tunisia.
Email: takwa.sellami@etu.u-cergy.fr

1. INTRODUCTION

Wind turbine systems control and diagnostic present one of the most challenging issues in academic researches area. Diagnostic strategies are based on setting up Fault Detection and Isolation (FDI) methods in order to establishan efficient fault tolerant control scheme. FDI methods are twisted to ensure the continuity of service under faulty conditions and to protect the system equipment [1].

A great deal of consideration has been devoted to observer-based FDI techniques [2]. Indeed, observers avoid the requirement for additional equipment and sensors to control the system under faulty conditions. Observer-FDI techniques are based on generating residuals sensitive to specific faults [3]. Once the fault is present, the indicators are alarmed as the residual exceeds its corresponding threshold.Sliding Mode Observers (SMO) are mostly adopted in the industrial diagnosis process, because they are robust means against system parametric variations [4]. Their main features are that they are able to compensate the faults impacts and to reconstruct the electrical and mechanical signals without stopping the service.

Three-phase induction machine drives are widely adopted in industrial applications, like electrical systems, traction drives, and especially in high-power variable-speed wind turbine systems. Typically, Indirect Rotor Flux Oriented Control (IRFOC) method controls Induction Generator (IG) by imposing its rotor flux. The method stability and robustness were proved for 5-phase induction motor with rotor resistance variation in [5]. The main advantage of this method is that it excludes the leakage reactance influence of both the stator and the rotor. Nevertheless, it has to be verified if this control scheme is sufficient to handle faults

presence or have tobe replaced by another more robust scheme. Indeed, results presented in [6] show that the spectrum of current components in field-oriented controlled machines has useful features in diagnostic procedure.

Inter-Turn Short-Circuit (ITSC) fault, usually triggered by partial discharge, is a critical fault affecting the stator windings of induction machines. Indeed, ITSC fault propagates rapidly in machines and grows to turn-turn or turn-ground short-circuit. Inter-turns short-circuit fault engenders additional mechanical stress and noise to the system [7]. Short–circuit fault can be destructive for the machine in a quick time [8]. In [9], the authors studied the electrical and mechanical signals of a doubly fed induction generatorunder short-circuit fault conditions. The results demonstrate that only in uncritical post-fault situations, wind turbines control schemes are able to restore the stability of the produced power without disconnections. Furthermore, the fault impact includes the converters and the transformer ensuring the grid-connection [10]. As a result, the stability of the power supplied to the grid can be disturbed.

Short-circuit faults modify the IG topology by changing its physical parameters [11]. Accordingly, the disturbed electrical and mechanical signalscarry important information about the fault. Stator currents are the machine signals the most affected by the ITSC fault. In fact, a recent study [12] of a 50 Hz 4 pole induction motor under healthy and faulty conditions assessed the increase in the backwards sequence current component. The study confirms that the negative sequence component is a powerful component for the detection of inter-turn faults. From here, SMO are called to reconfigure stator currents in order to detect and isolate the fault [13]-[14]. The basic idea of the proposed FDI method is to generate residuals via SMO able to captivate information about stator faults. The information will be then transmitted to indicators in order to trigger the alarms.

This paper is organized as follows: the wind turbine components models are presented in the second section. In the third section, ITSC fault affecting a wind turbine driven IG is developed using MATLAB/SIMULINK. Indeed, the fault impact on the electrical and mechanical signals of the variable-speed wind turbine are extracted. Stator currents are reconstructed in the following section using SMO. Afterwards, simulation results of the proposed FDI scheme are presentedunder both healthy and faulty conditions. Indeed, residuals are generated and compared to their thresholds in order to proclaim the ITSC detection and isolate the faulty phase. In the last section, conclusions are presented.

2. WIND TURBINE SYSTEM MODELLING

Within the progress in power-electronic converters technologies, connecting wind turbines to the grid power system, variable-speed wind turbines are nowadays increasing. These wind turbines capture an improved wind power and provide a better power quality than fixed-speed wind turbines. Figure 1 presents the schematic representation of the grid-connected wind turbine driven IG. The systemincludes a turbine, drive train, gearbox, IG, twoback-to-back converters and interface transformer. The two AC-DC-AC converters (stator-side converter and a grid-side converter) linked by a DC bus voltage (*E*), permit decoupling the generator electrical frequency from the grid frequency.

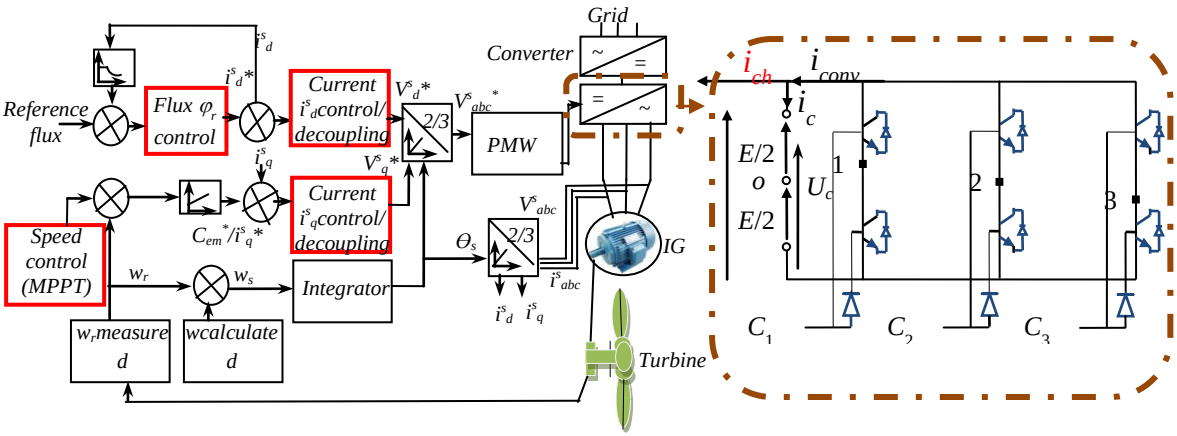

Figure 1. Schematic representation of the grid-connected wind turbine-driven IGcontrolled by IRFOC strategy

The essential points of interest of wind turbines driven IG are the ability to control the active and reactive grid-power (frequency and voltage control). Indeed, the grid-power control scheme controls the grid-side converter through feeding its Pulse Width-Modulated (PWM) by three-phase voltages reference. The control scheme also forces the bus voltage to follow its reference. The IG of the wind turbine system istypically controlled by indirect rotor flux orientedcontrol scheme. IRFOC method controls the stator-side converter through feeding its PWM by three-phase voltages reference [15].

2.1. Turbine Model

The turbine is characterized by an inertia $J_{turbine}$, a rotor radius R and a power coefficient C_p. C_p is calculated according to the pitch angle β and the tip speed ratio λ. The turbine is connected to a generator via a gearbox adapting the frequencies.The generator rotor is characterized by an inertia $J_g$and a coefficient of friction relative to the shaft f. The turbine accumulates a wind torque C_{ar}. Then, it transfers it to the gearbox. A torque $C_g$is then delivered from the gearbox to the generator. The generator rotating at the speed Ω_{mec}, generates an electromagnetic torque C_{em}. Subjected to the wind characterized by a speed V, The turbine tip speed-ratio $\lambda$is defined by

$$\lambda = \frac{R\Omega_{mec}}{V} \tag{1}$$

The turbine is defined by a total inertia J_t expressed by

$$J_t = \frac{J_{turbine}}{G^2} + J_g \tag{2}$$

The mechanical equation of the system is defined by

$$J_t \frac{d\Omega_{mec}}{dt} = C_{em} - C_g - f\Omega_{mec} \tag{3}$$

Where the torque C_g is defined by

$$C_g = \frac{C_{ar}}{G} = \frac{P_{ar}}{G\Omega_{mec}} = \frac{\frac{1}{2}\rho \pi R^2 V^3 C_p(\lambda,\beta)}{G\Omega_{mec}} \tag{4}$$

C_{ar} is the rotor aerodynamic torque. P_{ar} is the absorbed aerodynamic power. ρ is the air density of the air.

2.2. Induction Generator Model

The induction generator closed-loop model is set up in Park reference frame (d,q) following d (direct axis) and q (quadrature axis). Considering r^r and r^s the phase resistance of respectively the rotor and the stator of the p pairs of poles IG. L_s (stator inductance), L_r (rotor inductance) and M_{sr} (stator-rotor interaction inductance) are the IG parameters of the machine relative to (d,q)-reference frame. The cyclic mutual inductance between stator and rotor equivalent phases M(M=3/2 M_{sr}).

Considering θ_p is the rotating vector angle. θ_s is the rotating vector angle relative to the stator frame (synchronous speed). θ_s is the rotating vector angle relative to the rotor frame. The speeds ω_p, ω_s and ω_r are defined as the derivative of respectively the angles θ_p, θ_s and θ. ω_r is called the machine electric speed defined by $\omega_r = p\Omega_{mec}$, where Ω_{mec} is the machine mechanical speed. Applying Park transformation to the stator and rotor voltage Equations of the induction machine system becomes

$$\begin{cases} V^s{}_d = r^s i^s{}_d + \dfrac{d\varphi^s{}_d}{dt} - \omega_p \varphi^s{}_q \\ V^s{}_q = r^s i_{sq} + \dfrac{d\varphi^s{}_q}{dt} + \omega_p \varphi^s{}_d \\ 0 = r^r i^r{}_d + \dfrac{d\varphi^r{}_d}{dt} - \left(\omega_p - \omega\right)\varphi^r{}_q \\ 0 = r^r i^r{}_q + \dfrac{d\varphi^r{}_q}{dt} + \left(\omega_p - \omega\right)\varphi^r{}_d \end{cases} \quad (5)$$

The stator and rotor flux equations are defined by

$$\begin{cases} \varphi^s{}_d = L_s i^s{}_d + M i^r{}_d \\ \varphi^s{}_q = L_s i^s{}_q + M i^r{}_q \\ \varphi^r{}_d = L_r i^r{}_d + M i^s{}_d \\ \varphi^r{}_q = L_r i^r{}_q + M i^s{}_q \end{cases} \quad (6)$$

The machine produced electromagnetic torque C_{em} is expressed by

$$C_{em} = p\frac{M}{L_r}\left(\varphi^s{}_d i^s{}_q - \varphi^s{}_q i^s{}_d\right) \quad (7)$$

3.2. PWM Power Converter Model

The stator-side and grid-side converters ensure decoupling the electrical and the mechanical frequencies. The converter includes three legs as presented in Figure 1, each one features two-semiconductor switches with antiparallel connected freewheeling diodes. *E* being the DC bus voltage at the input of the voltage inverter. A PWM bloc feeds the converter. The two-semiconductor switches of the same leg are controlled via gate signals C_i (i= 1, 2, 3). The function C_i is a binary function representing the state of the i^{th} leg of the voltage converter. This function is sufficient on its own to characterize the operation of an entire leg. Indeed, the switches of the same leg are controlled in a complementary manner in order to avoid a short circuit of the input voltage source (U_c=E). Thus, the function $C_i$controlling the i^{th} leg is defined as follows

a. C_i=1 If the top switch is closed and the bottom switch is open
b. C_i=0 If the top switch is open and the bottom switch is closed.

For a balanced three-phase load, the case of a three-phase IG, the relation linking the voltage vectors $V^s{}_a$, $V^s{}_b$ and $V^s{}_c$ to the control signals C_1, C_2 and C_3 are given by the following matrix relationship

$$\begin{bmatrix} V^s{}_a \\ V^s{}_b \\ V^s{}_c \end{bmatrix} = \begin{bmatrix} V_{1N'} \\ V_{2N'} \\ V_{3N'} \end{bmatrix} = \frac{U_c}{3}\begin{bmatrix} 2 & -1 & -1 \\ -1 & 2 & -1 \\ -1 & -1 & 2 \end{bmatrix}\begin{bmatrix} C_1 \\ C_2 \\ C_3 \end{bmatrix} \quad (8)$$

The converter current output i_{ch}can then be calculated, after Laplace transformation, by

$$i_{ch} = i_{con} - CsU_c \quad (9)$$

Where C is the bus capacitor.

3. WIND TURBINE CONTROL SCHEME

3.1. Maximum Power Point Tracking (MPPT) Control

For every operating wind turbine, a maximum wind power can be tracked relatively to the turbine maximum power coefficient (C_{pmax}). Hence, for every wind profile, there is an optimum rotor speed

ensuringan optimal tip speed ratio λ_{opt}. Maximum Power Point Tracking (MPPT) techniques are developed while considering a fixed pitch angle β for extracting the maximum wind power. The developed MPPT scheme, presented in Figure 2, is based on controlling the rotor speed via PI controllers in order to ensure a maximum produced power.

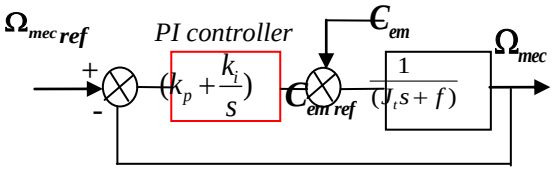

Figure 2. Control structure of the turbine speed

MPPT method is based on forcing the tip ratio λ to its maximum value λ_{opt}. The turbine speed reference is then calculated by

$$\Omega_{mec_{ref}} = \frac{V\lambda_{opt}}{R} \tag{10}$$

The coefficient $C_p$is then imposed to its maximum value C_{pmax}. Thus, he electromagnetic torque reference function is written by

$$C_{em_{ref}} = \frac{V\lambda_{opt}}{R}\frac{1}{2}\rho\,\pi \mathrm{R}^2\,V^3 C_{p\max} \tag{11}$$

To control the speed, Laplace Transformation is used. Neglecting the mechanical torque C_g, the speed equation becomes

$$\Omega_{mec} = \frac{C_{em}}{(J_t s + f)} \tag{12}$$

The PI controller function is written by

$$C(s) = k_p + \frac{k_i}{s} \tag{13}$$

K_p is the PI controller proportional-parameter controlling the system reply time. K_i is the PI controller integral-parameter controlling the overtaking. It is noted that the parameters values of the turbine speed PI controller are fixed according to desired performances (desired damping ratio ξ and natural frequency ω_0). A simple method for identifying these parameters (ξ and ω_0) for wind turbines is developed in [16].

3.2. Indirect Rotor Flux Oriented Control Scheme

Indirect Rotor Flux Oriented Control (IRFOC) is a well-used techniquefor IG control because it ensures an independent control of both decoupled rotor flux and torque. The scheme controls *d* and *q* stator current components based on imposing the rotor flux according to the *d*-axis as follows

$$\begin{cases} \varphi^r{}_d = \varphi_r \\ \varphi^r{}_q = 0 \end{cases} \tag{14}$$

Forcing the rotor flux ($\varphi^r{}_q = 0$), Laplace transformation of the decoupling equations leads to

$$\begin{cases} V^s{}_d = (r^s + s\sigma L_s) i^s{}_d + s\dfrac{M}{L_r}\varphi_r - \omega_s \sigma L_s i^s{}_q \\ V^s{}_q = (r^s + s\sigma L_s) i^s{}_q + \omega_s \dfrac{M}{L_r}\varphi_r + \omega_s \sigma L_s i^s{}_d \end{cases} \quad (15)$$

Developing the system equations, the control equations are then defined by

$$\begin{cases} \varphi_r = \dfrac{M}{1+\tau_r} i^s{}_d \\ C_{em} = p\dfrac{M}{L_r} i^s{}_q \\ \omega_r = \dfrac{M}{\tau_r \varphi_r} i^s{}_q \\ \omega_s = p\Omega_{mec} - \omega_r \end{cases} \quad (16)$$

To control the rotor flux and the stator currents, PI controllers are required. Figure 1 presents the IG close-loop based on IRFOC technique. Indeed, the imposed flux φ_r generates a reference current $i^s{}_d{}^*$. The PI controller of the current $i^s{}_d$ generates a reference voltage$V^s{}_d{}^*$. The PI controller of the current $i^s{}_q$ generates a reference voltage $V^s{}_q{}^*$. The speed PI controller, achieved by the MPPT technique, generates an electromagnetic torque reference $C_{em}{}^*$. The parameters of flux and currents PI-controllers are chosen using the division compensation technique, well described in [17], and according to the desired IG performances (desired damping ratio ξ and natural frequency ω_0).

It is noted that IRFOC scheme controls the stator-side converter. The technique generates three-voltage reference $V^s{}_{abc}{}^*$ used for Pulse Width-Modulated (PWM) feeding. The grid-side converter is also controlled by a PWM supplied by three-phase voltages reference $V^{grid}{}_{abc}{}^*$. The control scheme is described in [15]. A grid control scheme (active-reactive power control method) ensures the adjustment of DC bus voltage and generate the reference voltage $V^{grid}{}_{abc}{}^*$[18].

4. ITSC FAULT IMPACT

4.1. IG Model under ITSC fault

Winding faults modify the machine topology by changing its parameters. A detailed description of ITSC modelling is presented in [19]. The insulation failure in the windings caused by a short-circuit fault generates an insulation resistance r_f. A current $i_f$circulating in the resistance r_f, controls the severity of the fault. ITSC fault is considered occurring in the first phase s_1 characterized by N^s turns number. $N^s{}_f$ turns are considered short-circuited. s_1-phase is then divided in to a sub-winding healthy portion (as_1) and a sub-winding faulty portion (bs_1). The factor k_{cc} can be then defined by dividing $N^s{}_f$ by N^s ($k_{cc} = N^s{}_f / N^s$). $r^s{}_{1b}$and $L^s{}_{1b}$are considered as respectively resistance and self-inductance of faulty winding. $M_{1a,2}$ and $M_{1a,3}$ appear as mutual inductances between as_1 and respectively the windings $s_2$and s_3. $M_{1a,1b}$, $M_{1b,2}$ and $M_{1b,3}$ are respectively created as mutual inductances between $bs_1$and respectively as_1, s_2 and s_3. M_{sr1}, M_{sr2} appear as mutual inductances between the rotor and respectively as_1 and bs_1. M^s and M^r present respectively the stator mutual inductances and the rotor mutual inductance. The neutral is connected ($V_{NN'}$=0V). The two other phases (s_2 and s_3) resistance r^s and self-inductance L^s maintained not affected by the fault.For the rotor scheme, it is also not affected by the fault with a rotor phase resistance r^r and a self-inductance L^r. To study the ITSC fault, it is obligatory to develop the voltage equations in the (*abc*)-reference frame [19] defined by

$$\begin{cases} \left[V^s{}_{abcf}\right] = \left[R^s{}_{abcf}\right]\left[i^s{}_{abc}\right] + \left[L^{ss}{}_{abcf}\right]\dfrac{d}{dt}\left[i^s{}_{abcf}\right] + \dfrac{d}{dt}\left(\left[M^{sr}{}_{abcf}\right]\left[i^r{}_{abc}\right]\right) \\ \left[V^r{}_{abc}\right] = [0] = \left[R^r{}_{abc}\right]\left[i^r{}_{abc}\right] + \left[L^{rr}{}_{abc}\right]\dfrac{d}{dt}\left[i^r{}_{abc}\right] + \dfrac{d}{dt}\left(\left[M^{rs}{}_{abcf}\right]\left[i^s{}_{abcf}\right]\right) \end{cases} \quad (17)$$

Where the system voltage and current vectors are defined by

$[V^s_{abcf}]=\begin{bmatrix}V^s_a & V^s_b & V^s_c & 0\end{bmatrix}^T$, $[V^r_{abc}]=\begin{bmatrix}V^r_a & V^r_b & V^r_c\end{bmatrix}^T$, $[i^s_{abcf}]=\begin{bmatrix}i^s_a & i^s_b & i^s_c & i_f\end{bmatrix}^T$ and $[i^r_{abc}]=\begin{bmatrix}i^r_a & i^r_b & i^r_c\end{bmatrix}^T$

$$\left[R^s_{abcf}\right]=\begin{bmatrix} r^s & 0 & 0 & -r^s_{1b} \\ 0 & r^s & 0 & 0 \\ 0 & 0 & r^s & 0 \\ r^s_{1b} & 0 & 0 & -(r^s_{1b}+r_f) \end{bmatrix},\left[R^r_{abc}\right]=\begin{bmatrix} r^r & 0 & 0 \\ 0 & r^r & 0 \\ 0 & 0 & r^r \end{bmatrix},$$

$$\left[M^{sr}_{abcf}\right]=\begin{bmatrix} M_{sr}\cos(\theta) & M_{sr}\cos(\theta+\frac{2\pi}{3}) & M_{sr}\cos(\theta-\frac{2\pi}{3}) \\ M_{sr}\cos(\theta-\frac{2\pi}{3}) & M_{sr}\cos(\theta) & M_{sr}\cos(\theta+\frac{2\pi}{3}) \\ M_{sr}\cos(\theta+\frac{2\pi}{3}) & M_{sr}\cos(\theta-\frac{2\pi}{3}) & M_{sr}\cos(\theta) \\ -M_{sr_2}\cos(\theta) & -M_{sr_2}\cos(\theta+\frac{2\pi}{3}) & -M_{sr_2}\cos(\theta-\frac{2\pi}{3}) \end{bmatrix}$$

Where $\left[R^s_{abcf}\right]$, $\left[R^r_{abc}\right]$ and $\left[M^{sr}_{abcf}\right]$ present respectively the stator and rotor new parametric resistance and inductance matrices. $\left[L^{ss}_{abcf}\right]$ and $\left[L^{rr}_{abcf}\right]$ present respectively the stator and rotor new parametric inductance matrices defined

$$\left[L^{ss}_{abcf}\right]=\begin{bmatrix} L^s+l^s & M_{1a,2}+M_{1b,2} & M_{1a,3}+M_{1b,3} & -\left(L^s_{1b}+l^s_{1b}+M_{1a,1b}\right) \\ M_{1a,2}+M_{1b,2} & L^s+l^s & M^s & -M_{1b,2} \\ M_{1a,3}+M_{1b,3} & M^s & L^s+l^s & -M_{1b,3} \\ L^s_{1b}+l^s_{1b}+M_{1a,1b} & M_{1a,2} & M_{1a,3} & -\left(L^s_{1b}+l^s_{1b}\right) \end{bmatrix}, \left[L^{rr}_{abc}\right]=\begin{bmatrix} L^r+l^r & M^r & M^r \\ M^r & L^r+l^r & M^r \\ M^r & M^r & L^r+l^r \end{bmatrix}$$

4.2. ITSC Fault Impact on Wind Turbine System

In this section, we examine the stability of the system modules when the short-circuit fault appears. The simulations are realized using MATLAB/SIMULINK environment. We have applied a steady profile for wind (V=10m/s) over a period of 2s in order to focus on the ITSC fault impact. The tested system is characterized by a 14m-radius turbine. The turbine parameters are λ_{opt} = 5 and C_{pmax} = 0.44. It is connected to 11 kW IG rotating with 1450tr/min nominal speed. The tested IG is a machine of 4-poles, 50Hz frequency and 380/660V voltage. The IG load current is i^s_0 = 4A and the IG rated current i^s_n = 11.32A. It is characterized by stator turns number N^s = 48 and rotor turns number N^r = 32. The stator resistance $r^s$and inductance L^s are respectively 1.5Ω and 0.14H. The rotor resistance r^r and inductance L^r are respectively 0.7Ω and 0.28H.

First, no short-circuited turns are presented. Then, at the instant *t=1*.5s, ITSC fault is introduced. In fact, 30% of the turns of the first phase (s_1) are short-circuited (k_{cc}=0.3). r_f was fixed to 0Ω due to the quick decrease of the insulation resistance r_f in most machine materials [20]. Figure 3 presents the simulation results of the outputs signals of the studied control schemes. The mechanical speed Ω_{mec} and its reference Ω_{mec}^* elaborated by the MPPT technique is plotted while applying the ITSC fault at t=1.5s (Figure 3(a)). Figure 3(b) presents the rotor flux (φ_r) and its reference elaborated by the IRFOC method. The currents control of stator currents (i^s_d, i^s_q) and their references ($i^{s}_{d}{}^*$, $i^{s}_{q}{}^*$) are presented by respectively Figure 3(c) and Figure 3(d). It can be seen that fluctuations appear in the control outputs once the fault is present. Indeed, short-circuit fault leads to a significant instability of IRFOC scheme outputs.

Three-phase stator currents and voltages contain important information about stator faults. Time-domain signatures analysis is a good tool for evaluating ITSC fault impacts. Thus, Figure 3(e) and Figure 3(f) present the supplied stator three-phasevoltage (V^s_a, $V^s_b$and V^s_c). It is noticed that, the stator voltages are balanced under healthy conditions ([0...1.5s] interval). However, once ITSC fault takes a place, an unbalance appears. The magnitude of the stator faulty voltage V^s_a decreases. However, the magnitude of the two-phase voltages (V^s_b andV^s_c) increase.

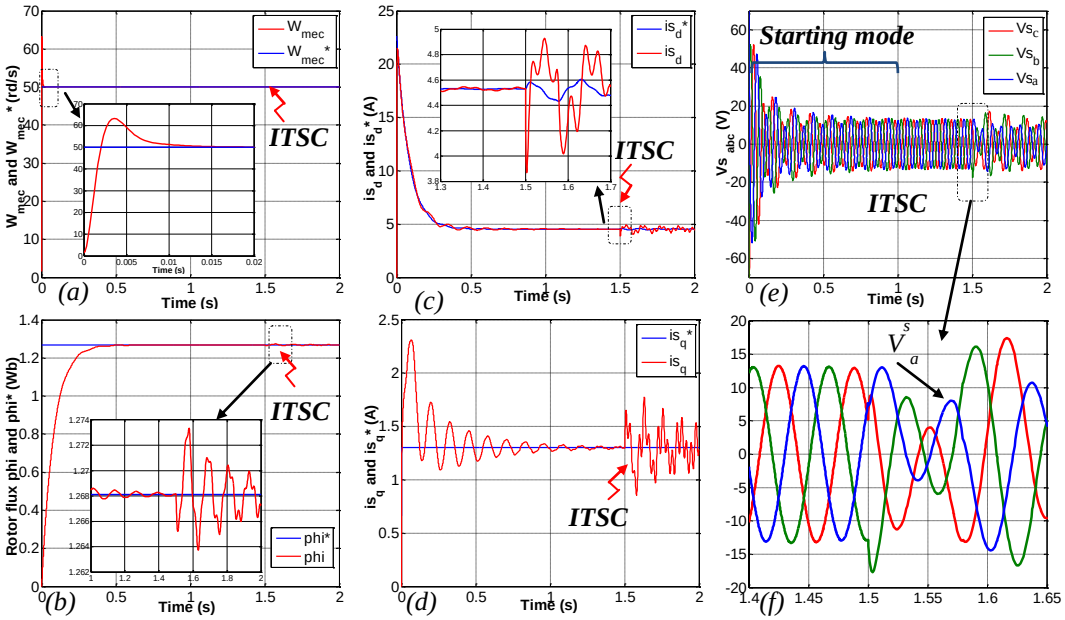

Figure 3. Simulation results of (a) mechanical speed Ω_{mec} and its reference Ω_{mec}^{*}, (b) estimated rotor flux $\varphi_r$and its reference φ_r^{*}, (c) current i^s_d and its reference $i^s_d{}^{*}$, (d) current $i^s_q$and its reference $i^s_q{}^{*}$, (e) three-phase stator voltages V^s_{abc} and (f) and their zooms at t = 1.5s of wind turbine IG with ITSC fault of 30% of s_1-phase

Figure 4(a) and Figure 4(b) present the stator three-phase currents (i^s_a, $i^s_b$and i^s_c). It is noticed that, stator currents are imbalanced in faulty machines ([1.5s...2s] interval). The current i^s_a, circulating in the faulty phase (s_1), rises significantly at t=1.5s. The other two-phase currents (i^s_b andi^s_c) also increase but with lower magnitudes compared to i^s_a magnitude. This result can be used to identify the faulty phase in FDI schemes.

It is also noted that the aim of control schemes is to ensure the stability between the system components. However, the fluctuations of the IG electromagnetic torque C_{em} presented in Figure 4(c) are reflected on the power quality delivered to the grid (Figure 4(d)). Figure 4(e) and Figure 4(f) show that instability oscillations appear in the stator-side converter output current i_{ch}. It can be deducted that the fault impact affects the stability of the grid-connection equipment starting with stator-side converter. As a result, the injected power to the grid P is disturbed.

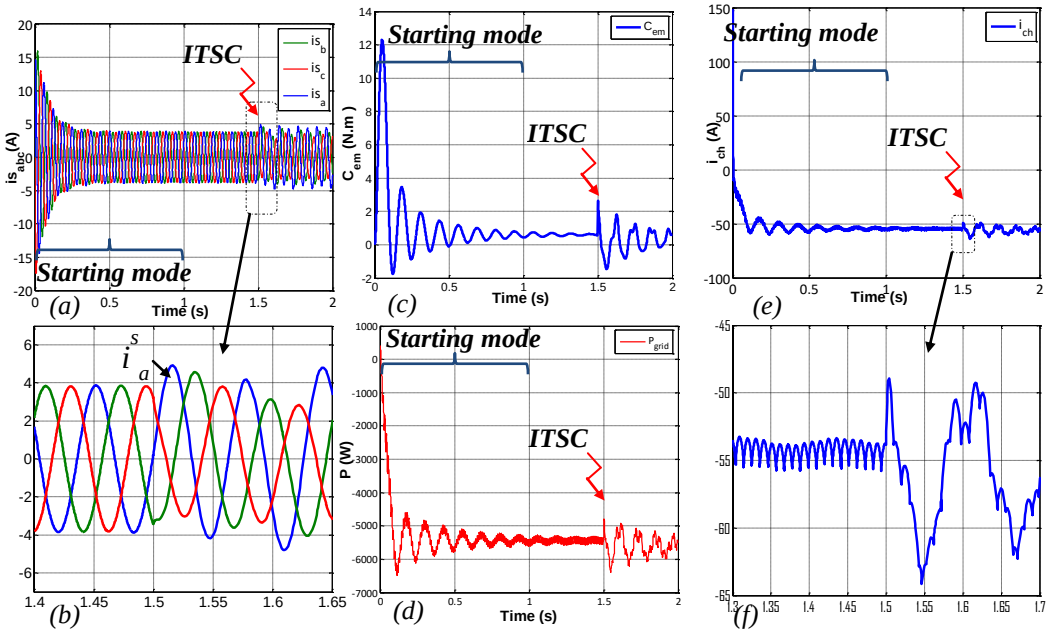

Figure 4. Simulation results of (a)) three-phase stator currents i^s_{abc}, (b) their zooms, (c) the electromagnetic torque C_{em}, (d) the supplied power P to the grid, (e) stator-side converter current i_{ch} and (f) its zoom at t=1.5s of wind turbine IG with ITSC fault of 30% of s_1-phase

5. FAULT DETECTION AND ISOLATION SCHEME

The proposed FDI scheme in this study is based on the results of the previous section. The observed fluctuations in the three-phase stator currents will be involved in residuals generation based on SMO. Then the residuals analysis will allow detecting the ITSC fault and isolate it [21]. Figure 5 presents the SMO-based fault detection and isolation scheme.

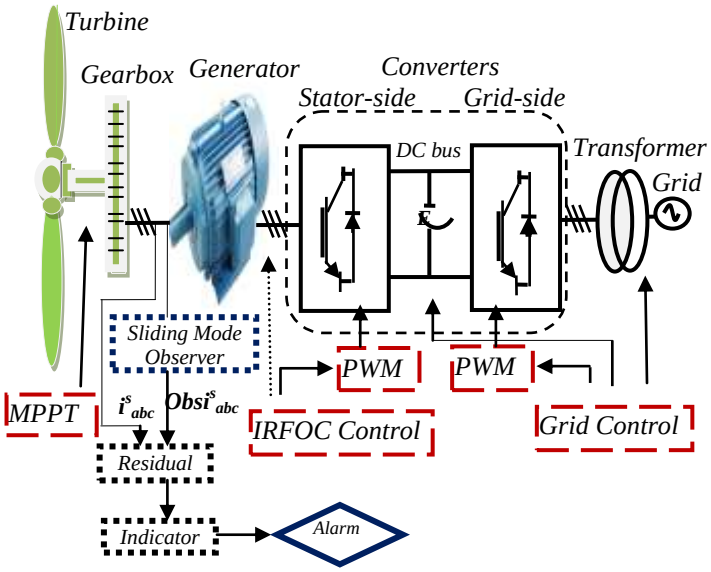

Figure 5. SMO-based fault detection and isolation method for wind turbine driven induction generator closed-loop system

5.1. Sliding Mode Observers Development

The aim of this section is to develop sliding mode observers able to compensate stator fault impacts. SMO recreate stator currents not affected by the fault thanks to Lyapunov theory [22]. In fact, Lyapunov function ensures the system closed-loop stability. It forces the signals to follow their references despite the faults presence [23]. The five-order nonlinear system of the IG can be described in the stator (*αβ)*-stationary reference by

$$\begin{cases}\left[X^{\square}\right]=[A][X]+[B][U] \\ [Y]=[C][X]\end{cases} \tag{18}$$

Where the input, output and state vectors are defined by

$$[U]=\left[V^s{}_\alpha \quad V^s{}_\beta\right]^T,\ [Y]=\left[i^s{}_\alpha \quad i^s{}_\beta\right]^T \text{ and } [X]=\left[i^s{}_\alpha \quad i^s{}_\beta \quad \varphi^r{}_a \quad \varphi^r{}_\beta\right]^T$$

The matrices *A*, *B* and *C* are defined as follows

$$A=\begin{bmatrix}-a_1 & 0 & a_3 & a_2\omega \\ 0 & -a_1 & -a_2\omega & a_3 \\ a_5 & 0 & -a_4 & -\omega \\ 0 & a_5 & \omega & -a_4\end{bmatrix};\ B=\begin{bmatrix}b & 0 \\ 0 & b \\ 0 & 0 \\ 0 & 0\end{bmatrix};\ C=\begin{bmatrix}1 & 0 & 0 & 0 \\ 0 & 1 & 0 & 0\end{bmatrix}$$

a_i (*i*=1,..,8) and *b* are the system parameters defined by

$$a_1=\left(\frac{1}{\sigma\tau_s}+\frac{1-\sigma}{\sigma\tau_r}\right),\ a_2=\frac{1-\sigma}{\sigma M_{sr}},\ a_3=\frac{1-\sigma}{\sigma M_{sr}\tau_r},\ a_4=\frac{1}{\tau_r},\ a_5=\frac{M_{sr}}{\tau_r},\ a_6=\frac{P^2M_{sr}}{J_gL_r},\ a_7=\frac{f}{J_g},\ a_8=\frac{P}{J_g},$$

$$b=\frac{1}{\sigma L_s},\ \sigma=1-\frac{M_{sr}{}^2}{L_sL_r},\ \tau_s=\frac{L_s}{r^s},\ \tau_r=\frac{L_r}{r^r}.$$

SMO equations system are defined by

$$\begin{cases}\left[\hat{X}^{\square}\right]=[A]\left[\hat{X}\right]+[B]\left[\hat{U}\right]+\lambda\,\mathrm{sgn}(S_i) \\ \left[\hat{Y}\right]=[C][\hat{X}]\end{cases} \tag{19}$$

Where the parametric vector λ is written by

$\lambda=[\lambda_1, \lambda_2, \lambda_3, \lambda_4]^T$ where $[\lambda_1]=[\lambda_{11}\lambda_{12}]$, $[\lambda_2]=[\lambda_{21}\lambda_{22}]$, $[\lambda_3]=[\lambda_{31}\lambda_{32}]$ and $[\lambda_1]=[\lambda_{41}\lambda_{42}]$.

To estimate the stator currents and rotor flux dynamics errors, estimated errors e_i (*i*=1..4) are defined by

$$\begin{cases}e_1=i^s{}_\alpha-\hat{i}^s_\alpha \\ e_2=i^s{}_\beta-\hat{i}^s_\beta \\ e_3=\varphi^r{}_\alpha-\hat{\varphi}^r_\alpha \\ e_4=\varphi^r{}_\beta-\hat{\varphi}^r_\beta\end{cases} \tag{20}$$

S_i (*i*=1,2) carry the difference between measured and observed stator currents. It is defined by

$$\begin{cases}S_1=e_1=i^s{}_\alpha-\hat{i}^s_\alpha \\ S_2=e_1=i^s{}_\beta-\hat{i}^s_\beta\end{cases} \tag{21}$$

Defining then the slidingsurface *S* by

$$S=\begin{bmatrix}S_1\\S_2\end{bmatrix}=Q\begin{bmatrix}e_1\\e_2\end{bmatrix} \tag{22}$$

Where the parametric matrices are supposed to be [19]

$$Q^{-1}=\begin{bmatrix}\lambda_{11} & \lambda_{12}\\ \lambda_{31} & \lambda_{32}\end{bmatrix}=\begin{bmatrix}a_3 & a_2\omega\\ -a_2\omega & a_3\end{bmatrix} \tag{23}$$

Lyapunov condition imposesthe following equation

$$V=\frac{S^TS}{2} \tag{24}$$

The derivative of Lyapunov function is then expressed by

$$\dot{V}=S^TQ\begin{bmatrix}\dot{e}_1\\ \dot{e}_2\end{bmatrix}+S^T\dot{Q}\begin{bmatrix}e_1\\e_2\end{bmatrix} \tag{25}$$

Respecting the attractivity conditions, γ_1 and γ_2 are calculated [19]. Developping the system equations, the SMO parameters vector λ can be finally calculated by

$$\begin{bmatrix}\lambda_{21} & \lambda_{22}\\ \lambda_{41} & \lambda_{42}\end{bmatrix}=\begin{bmatrix}q_1 & 0\\ 0 & q_2\end{bmatrix}\begin{bmatrix}\gamma_1 & 0\\ 0 & \gamma_2\end{bmatrix} \tag{26}$$

Where the parametric vector λ_i(i=1…4) are defined by

$$\begin{cases}\lambda_1=\begin{bmatrix}a_2.\gamma_1 & a_3.\omega.\gamma_2\end{bmatrix}\\ \lambda_2=\begin{bmatrix}q_1\gamma_1 & 0\end{bmatrix}\\ \lambda_3=\begin{bmatrix}-a_3.\omega.\gamma_1 & a_2.\gamma_2\end{bmatrix}\\ \lambda_4=\begin{bmatrix}0 & q_2\gamma_2\end{bmatrix}\end{cases} \tag{27}$$

5.2. Residuals Generation

The basic idea of observed-based FDI technique is to generate residuals carrying the difference between measured and reconstructed outputs [24]-[25]. Under healthy conditions, a residual is close to zero and it diverges significantly under faulty conditions. The IG currents thresholds are fixed under healthy conditions and steady parametric variations. Indeed, currents thresholds are calculated according to the healthy tested IG boundary parametric variations. When residuals exceed thresholds, an alarm is triggered to indicate the detection of the fault. $Tis_{a,}$ Tis_b and Tis_c present the three thresholds for respectively the three stator currents $i^s{}_a$, $i^s{}_b$ and $i^s{}_c$. Their corresponding residuals are respectively $Ris_{a,}$ Ris_b and $Risc$. Expressions of residuals relative to the IG stator currents are defined by

$$\begin{cases}Ris_a=i^s{}_a-\hat{i}^s_a\\ Ris_b=i^s{}_b-\hat{i}^s_b\\ Ris_c=i^s{}_c-\hat{i}^s_c\end{cases} \tag{28}$$

The fault indicators I_1, I_2 and I_3 will catch the overtaking of residuals (Ris_{a_max}, Ris_{b_bmax} and Ris_{c_max}). I_1, I_2 and I_3 are then defined by

$$\begin{cases} I_1 = Ris_{a\_\max} - T\,is_a \\ I_2 = Ris_{b\_\max} - T\,is_b \\ I_3 = Ris_{c\_\max} - T\,is_c \end{cases} \quad (29)$$

The function I_i (i=1,2,3) will announce the fault presence using a fault alarm signal *FD* as follows

a. *FD*=1 if I_i (i=1,2,3) > 0(the fault is declared)
b. *FD*=0 if I_i (i=1,2,3) < 0(no fault is declared).

The last phase of the FDI scheme is the isolation of the faulty phase. Thus, three fault-alarm signals *FI1*, *FI2* and *FI3* are defined. The ITSC fault isolation scheme is given by the following algorithm

a. *FI1*=1, *FI2*=0 and *FI3*=0 if $I_{1=}$ max (I_1,I_2,I_3)
b. *FI2*=1, *FI1*=0 and *FI3*=0 if $I_{2=}$ max (I_1,I_2,I_3)
c. *FI3*=1, *FI1*=0 and *FI2*=0 if $I_{3=}$ max (I_1,I_2,I_3)

Accordingly, the fault-alarm signal *FIk*, (*k*=1,2,3) deviates from 0 to 1 when the k^{th} phase is affected by ITSC fault.

5.3. Fault Detection and Isolation

The aim of this section is to investigate the robustness of SMO-based FDI method under ITSC faults. The SMO-reconstructed three-phase currents ($\hat{i}_a^s$, $\hat{i}_b^s$ and $\hat{i}_c^s$) are presented in Figure 6(a). The three-phase stator measured currents $i^s_{abc}$are also presented in Figure 6(b).Comparing the measured and observed currents, it can be noticed that at the instant of appearance of the ITSC fault, the three reconstructed currents start to be imbalanced just like measured ones. Then, the SMO restore the equilibrium after 0.2s (at *t*=1.7s). It can be then deducted that SMO are able to compensate ITSC fault impacts and reconstruct quickly three-phase stator currents insensitive to the fault presence. The reconstructed currents allow generating efficient residuals for detecting the stator fault.

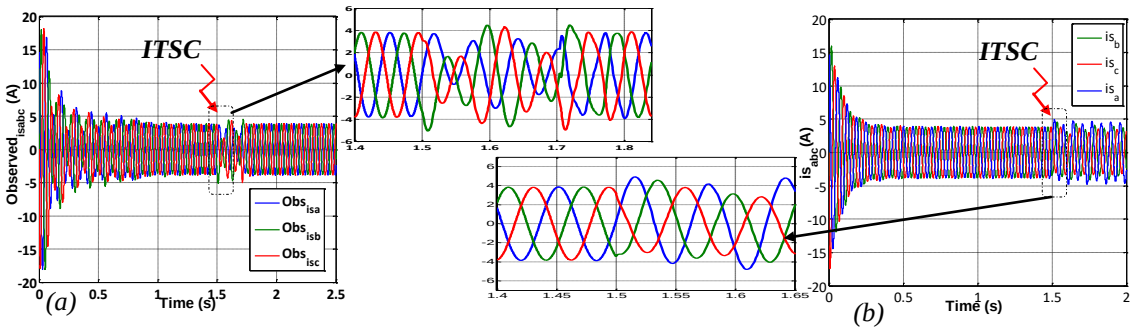

Figure 6. Simulation results of (a) three-phase stator SMO reconstructed currents $\hat{i}^s_{abc}$ and (b) measured currents i^s_{abc} with their zooms at *t*=1.5s of wind turbine system IG with ITSC fault of 30% of s_1-phase

The currents residuals and their corresponding thresholds Tis_a, Tis_b and Tis_c are collected in Figure 7. Tis_a, Tis_b and Tis_c magnitudes of the IG under test are fixed to 1A based on simulation results under healthy conditions and operating resistance variations. The IG operates in the starting mode until 1s. Thus, the FDI method takes 1s to operate until the residuals convergence.It can be seen that the residuals exceed the thresholds at *t*=1.6s because of the ITSC fault presence. The indicators I_i (*i*=1,2,3) are then loaded (I_1=2.2A, I_1=2A and I_3=1A). As a result, the fault alarm signal FD changes from 0 to 1. The highest magnitude of indicators (I_1) corresponds to the stator phase affected by the ITSC (s_1-phase). Thus, only the fault-alarm signal *FI1* deviates from0to1. *FI1* declares that the 1^{st} phase (s_1) is suffering from an ITSC fault.

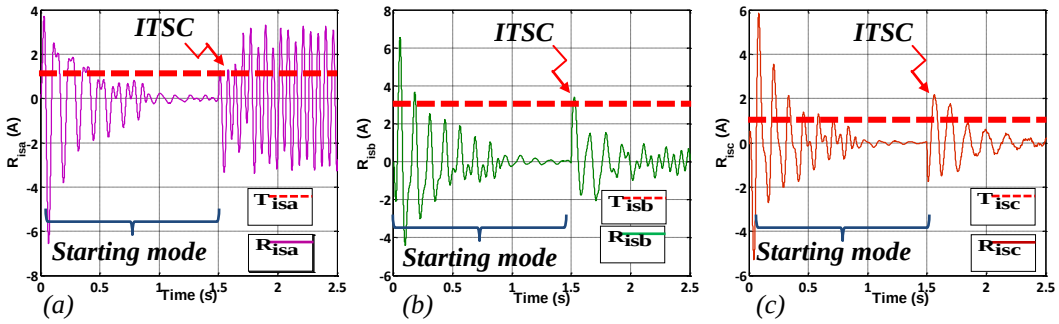

Figure 7. Simulation results of (a) residual $Ris_a$and its thresholds Tis_a, (b) residual $Ris_b$and its thresholds Tis_b and (c) residual $Ris_c$and its thresholds $Tis_c$of wind turbine IG with ITSC fault of 30% of s_1-phase

6. CONCLUSION

In this paper, an accurate closed-loop model of a variable-speed grid-connected wind turbine was set up. Afterward, inter-turn short-circuit fault impacts on electrical and mechanical signals of the system are investigated. It has been realized that, once the fault appears the stator currents are disturbed engendering perturbations in the stator-side converter input voltages and output currents. Hence, the stability of the supplied power to the grid is fluctuated which highlights the requirement of an efficient fault detection and isolation scheme. A robust SMO-based fault detection and isolation method is then developed. Indeed, the method is established through generating residuals carrying appropriate information about the stator fault. Furthermore, the affected phase is isolated quickly in order to ensure providing a continuous supply of stable power to serve the grid.The developed method shows its efficacy and quickness in detecting short-circuit faults and isolating the faulty phase. However, the system has to switch to a fault tolerant control scheme once the FDI technique detects the fault, which will be the aim of our future study.

ACKNOWLEDGEMENTS

This research project was supported by the both Tunisian and French Ministries of High Education and Scientific Research.

REFERENCES

[1] M. Blanke, *et al*., "Diagnosis and fault-tolerant control", *Berlin: springer*, (Vol. 691), 2006.
[2] P. M. Frank and X. Ding, "Survey of robust residual generation and evaluation methods in observer-based fault detection systems", *Journal of process control*, 7(6), 403-424, 1997.
[3] H. Li, *et al*., "Observer-based fault detection for nonlinear systems with sensor fault and limited communication capacity", *IEEE Transactions on Automatic Control*, 61(9), 2745-2751, 2016.
[4] C. Edwards, *et al*., "Sliding mode observers for fault detection and isolation", *Automatica*, 36(4), 541-553, 2000.
[5] H. Echeikh, M. F. Mimouni, *et al*., "Comparative study between the rotor flux oriented control and non-linear backstepping control of a five-phase induction motor drive–an experimental validation", *IET Power Electronics*, 9(13), 2510-2521, 2016.
[6] A. Bellini, *et al*., "Closed-loop control impact on the diagnosis of induction motors faults", *IEEE transactions on Industry Applications*, 36(5), 1318-1329, 2000.
[7] S. T. WAN, *et al*., "Analysis of generator vibration characteristic on stator winding inter-turn short circuit fault [J]", *Proceedings of the Csee*, 4, 2004.
[8] S. Toumi, M. F. Mimouni, *et al*., "Modeling and Simulation of a PMSG-based Marine Current Turbine System under Faulty Rectifier Conditions", *Electric Power Components and Systems*, 45(7), 715-725, 2017.
[9] D. Shah, *et al*., "Stator-interturn-fault detection of doubly fed induction generators using rotor-current and search-coil-voltage signature analysis", *IEEE Transactions on Industry Applications*, 45(5), 1831-1842, 2009.
[10] H. M. Abdel-Mageed, "Simulation of the different transmission line faults for a grid connected wind farm with different types of generators", *International Journal of Electrical and Computer Engineering*, 2(1), 35, 2012.
[11] F. Wu, *et al*., "Analytical Modeling of Inter-turn Short Circuit for Multiphase Fault-Tolerant PM Machines with Fractional Slot Concentrated Windings", *IEEE Transactions on Industry Applications*, 53(3), 1994-2006, 2017.
[12] D. G. Dorrell and K. Makhoba, "Detection of Inter-turn Stator Faults in Induction Motors Using Short Term Averaging of Forwards and Backwards Rotating Stator Current Phasors for Fast Prognostics", *IEEE Transactions on Magnetics*, 2017.
[13] A. Hosseyni, M. F. Mimouni, *et al*., "New Sensorless Sliding Mode Control of a Five-Phase Permanent Magnet Synchronous Motor Drive Based on Sliding Mode Observer", *International Journal of Power Electronics and Drive Systems*, 8(1), 184, 2017.

[14] S. Krim, M. F. Mimouni, *et al*., "FPGA-Based Implementation Direct Torque Control of Induction Motor", *International Journal of Power Electronics and Drive Systems*, 5(3), 293, 2015.
[15] T. Sellami, *et al*., "Impact of Inter-Turn Short-Circuit Fault on Wind Turbine Driven Squirrel-Cage Induction Generator Systems", In *Conférence Internationale en Sciences et Technologies Electriques au Maghreb CISTEM 2014, November* 2014.
[16] T. Sellami, M. F. Mimouni, Modal and harmonic analysis of three-dimensional wind turbine models. *Wind Engineering*, 40(6), 518-527, 2016.
[17] K. H. Ang, et al., "PID control system analysis, design, and technology", *IEEE transactions on control systems technology*, 13(4), 559-576, 2005.
[18] L. Xu and P. Cartwright, "Direct active and reactive power control of DFIG for wind energy generation", *IEEE Transactions on energy conversion*, 21(3), 750-758, 2006.
[19] T. Sellami, M. F. Mimouni, "Sliding mode observer-based fault-detection of inter-turn short-circuit in induction motor", In *Sciences and Techniques of Automatic Control and Computer Engineering (STA), 2013 14th International Conference on* (pp. 524-529). IEEE, December 2013.
[20] Q. F. Lu, *et al*., "Model of stator inter-turn short circuit fault in doubly-fed induction generators for wind turbine", In *Power Electronics Specialists Conference, 2004. PESC 04. 2004 IEEE 35th Annual* (Vol. 2, pp. 932-937). IEEE, June 2004.
[21] A. Hosseyni, A., M. F. Mimouni, *et al*., "An improved sensorless sliding mode control/adaptive observer of a five-phase permanent magnet synchronous motor drive", *The International Journal of Advanced Manufacturing Technology*, 1-11, 2017.
[22] J. A. Moreno and M. Osorio, "A Lyapunov approach to second-order sliding mode controllers and observers", In *Decision and Control, 2008. CDC 2008. 47th IEEE Conference on* (pp. 2856-2861). IEEE, December 2008.
[23] A. Derdiyok, *et al*., "Design and implementation of a new sliding-mode observer for speed-sensorless control of induction machine", *IEEE Transactions on Industrial Electronics*, 49(5), 1177-1182, 2002.
[24] S. Krim, M. F. Mimouni, *et al*., "Implementation on the FPGA of DTC-SVM Based Proportional Integral and Sliding Mode Controllers of an Induction Motor: A Comparative Study", *Journal of Circuits, Systems and Computers*, 26(03), 1750049, 2017.
[25] T. Sellami,*et al*.,"3D Finite Volume model for free and forced vibrations computation in on-shore wind turbines", In *Sciences of Electronics, Technologies of Information and Telecommunications (SETIT), 2016 7th International Conference on* (pp. 104-108). IEEE, December 2016.